# Humanoid-Human Sit-to-Stand-to-Sit Assistance

Hugo Lefèvre, Tomohiro Chaki, Tomohiro Kawakami, Arnaud Tanguy, Takahide Yoshiike, Abderrahmane Kheddar

# Humanoid-Human Sit-to-Stand-to-Sit Assistance

Hugo Lefèvre[1], Tomohiro Chaki[2], Tomohiro Kawakami[2], Arnaud Tanguy[1], Takahide Yoshiike[2], Abderrahmane Kheddar[3], *Fellow, IEEE*

***Abstract*—Standing and sitting are basic tasks that become increasingly difficult with age or frailty. Assisting these movements using humanoid robots is a complex challenge, particularly in determining where and how much force the robot should apply to effectively support the human's dynamic motions. In this letter, we propose a method to compute assistive forces directly from the human's dynamic balance, using criteria typically employed in humanoid robots. Specifically, we map humanoid dynamic balance metrics onto human motion to calculate the forces required to stabilize the human's current posture. These forces are then applied at the appropriate locations on the human body by the humanoid. Our approach combines the variable height 3D divergent component of motion with gravito-inertial wrench cones to define a 3D balance region. Using centroidal feedback, we compute the required assistance force to maintain balance and distribute the resulting wrenches across the human's body using a humanoid robot dynamically balanced according to the same criteria. We demonstrate the effectiveness of this framework through both simulations and experiments, where a humanoid assists a person in sit-to-stand and stand-to-sit motions, with the person wearing an age-simulation suit to emulate frailty.**

***Index Terms*—humanoids, human assistive humanoids, dynamic balance criteria, multi-body motion control.**

## I. Introduction

CLOSE-PHYSICAL interactions between humans and humanoids hold significant promise for assisting frail and elderly individuals. Given the rapid advancements in humanoid robotics, it is increasingly plausible that humanoids may play a central role in providing in-home assistance to people with limited mobility in the future. A representative scenario for this vision is a humanoid helping an individual to stand up or sit down —an example that captures the essence of the challenges ahead. To perform such tasks effectively, a humanoid must possess various interrelated capabilities (this list is not exhaustive): (i) the ability to position itself appropriately and establish contact with the person to provide assistance; (ii) continuous tracking of the person's posture and movement, as well as the location of supports in the surrounding environment; (iii) the ability to maintain the balance of both the human and humanoid during multi-contact interactions, accounting for possible changes in contact during the motion; (iv) the ability to apply forces to assist the person in achieving the intended motion. Other aspects are outlined in Sec. VI.

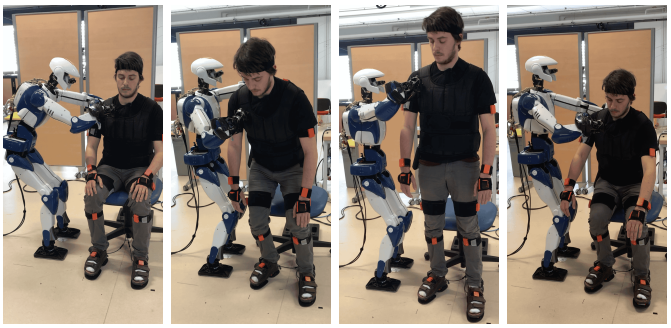

**Figure 1:** HRP-4 assisting a human standing-up and sitting again.

Item (i) is not the focus of this work and has been addressed in [1], [2]. In brief, guidelines in geriatric care provide recommendations for caregivers on how to position themselves and where to offer support through physical contact with patients, depending on the specific task at hand. A humanoid, with its anthropomorphic shape, would be well-suited to adhere to these recommendations. Item (ii) is assumed readily available, as discussed in Sec. IV-A. Item (iii) represents a key challenge. Although human balance has been extensively studied using force measurements and motion capture (e.g., [3], [4]), these methods generally rely on simplified criteria. In contrast, static and dynamic balance are well-explored in the context of humanoid bipedal locomotion control and planning, an area that is considerably more mature. A brief overview of existing methods is provided in Sec. II. The most complex challenge lies in computing the assistive forces and the resulting motion. To illustrate the difficulty, consider a simplified case involving a point mass $m$, which can generate a force $f_{\text{inner}}$ along the $x$-axis. To move from an initial position $x_0$ to a target position $x_t$, a specific force is required according to the dynamic equation $\ddot{x}$. If $f_{\text{inner}}$ is insufficient, it must be supplemented by an additional force $f_{\text{assist}}$, as given by the following equation:

$$m\ddot{x} = f_{\text{inner}} + f_{\text{assist}} \tag{1}$$

In this analogy, $m$ represents the person's weight (at the center of mass), $\ddot{x}$ is the acceleration of this center of mass, $f_{\text{inner}}$ is the force the person can exert through their own muscles, and $f_{\text{assist}}$ is the force that the robot must provide. The challenge for the humanoid lies in the fact that it does not have direct access to the desired dynamics of $\ddot{x}$, nor does it know the exact value of $f_{\text{inner}}$. Overestimating $f_{\text{inner}}$ can result in insufficient assistance, while underestimating it can disrupt the person's motion, both of which can lead to undesirable

Manuscript received July 5, 2024; Revised November 13, 2024; Accepted December 7, 2024

This paper was recommended for publication by Editor Angelika Peer upon evaluation of the Associate Editor and Reviewers' comments.

This work was supported by Collaborative Grant from Honda R&D Co Japan.

Contact author: A. Kheddar

[1]H. Lefèvre and A. Tanguy are with the CNRS-University of Montpellier, LIRMM, Montpellier, France.

[3]A. Kheddar is with the CNRS-AIST Joint Robotics Laboratory, IRL3218, Tsukuba, Japan, and with the CNRS-University of Montpellier, LIRMM, Montpellier, France.

[2]T. Chaki, T. Kawakami, T. Yoshiike are with Honda R&D Co., Ltd., 8-1 Hon-cho, Wako, Saitama, Japan.

Digital Object Identifier (DOI): see top of this page.

outcomes. This is why we refer to the optimal amount of $f_{\text{assist}}$ as the "synergistic force." This issue is relevant not only for humanoid assistance but also for other human-robot physical interaction, such as exoskeletons. Several approaches to computing $f_{\text{assist}}$ have been proposed, including model-based adaptive control and machine learning (see Sec. II).

In this letter, we propose a novel approach to computing $f_{\text{assist}}$ in a closed-loop fashion. Since sit-to-stand and stand-to-sit motions are dynamic, our method focuses on computing the assistive force that best ensures the dynamic balance of the person during these motions.

Our approach links items (iii) and (iv) from the previous list. To enforce the balance of both the human and humanoid during multi-contact assistance, we leverage advanced techniques commonly used in humanoid dynamic balance control and apply them to the human-humanoid dyad. Specifically, we combine robust static balance regions with the 3D divergent component of motion (DCM) (Sec. III-A) to assess whether the person is in dynamic balance while being assisted. The assistive force ($f_{\text{assist}}$) is then computed to adjust the DCM when it falls outside the computed balance region, using the virtual repellent point (VRP) and the external forces exerted by the person on the environment (Sec. III-C). While dynamic balance parameters can be directly measured using sensors and observers on the humanoid, these must be estimated for the human. This is achieved through motion capture (Sec. IV-A) and the use of force sensors worn by the person (Sec. IV-B). The robot then applies the computed assistive force to the person (Sec V-A) while also ensuring its own dynamic balance, similar to the way a caregiver would maintain balance during physical assistance (Sec. V-B).

We evaluate our method with three humanoids: Honda's E2-DR and Kawasaki's Friend in simulation, and the HRP-4 in real experiments assisting with sit-to-stand and stand-to-sit motions. To simulate frailty, the three human participants wore a commercially available age-simulation suit[1]. Our results show that the humanoid is capable of compensating for the lack of human strength in these motions, as illustrated in Fig 1. Additionally, participants were asked to reach the limits of their balance to test the humanoid's ability to apply forces that restore them to a stable position (Sec. VI). We have integrated the proposed method into our multi-robot whole-body QP open framework, `mc_rtc`[2] (Sec. IV).

## II. Background and Related Works

Several approaches exist for humanoid-human physical assistance (see Table I). In contrast to existing work, we propose an automated assessment of whether a person needs help, and exactly how much. Our algorithm computes dynamic balance criteria for persons to be assisted based on those used in humanoids, which has not been done before and explained hereafter.

### A. 3D Robust static balance region

Let $\boldsymbol{c} \in \mathbb{R}^3$ be the CoM position and $m$ the mass of a humanoid under $n$ unilateral contact points. For each contact $i$, let $\mathbf{r}_i \in \mathbb{R}^3$ be its contact position, $\mathbf{u}_i \in \mathbb{R}^3$ its normal, $\boldsymbol{f}_i, \boldsymbol{n}_i \in \mathbb{R}^3$ the force and moment applied at the contact and $\mu_i$ its friction coefficient, $\mathbf{g}$ the gravity vector, $\boldsymbol{L} \in \mathbb{R}^3$ the CoM angular momentum. The Newton-Euler equations governing the CoM motion write,

$$\sum_{i=1}^{n} \boldsymbol{f}_i + m\mathbf{g} = m\ddot{\boldsymbol{c}} \quad \text{and} \quad \sum_{i=1}^{n} (\mathbf{r}_i - \boldsymbol{c}) \times \boldsymbol{f}_i + \boldsymbol{n}_i = \dot{\boldsymbol{L}} \tag{2}$$

Unilateral contacts with non–slippage condition add:

$$\mathbf{u}_i^T \boldsymbol{f}_i \geq 0 \ \text{ and } \ \|(\mathbb{I} - \mathbf{u}_i \mathbf{u}_i^T)\boldsymbol{f}_i\| \leq \mu_i \mathbf{u}_i^T \boldsymbol{f}_i \tag{3}$$

Static balance regions ($\ddot{\boldsymbol{c}} = \mathbf{0}$) are computed efficiently in [8]. Another multi-contact criterion for balance enforces the contact resultant wrench to remain in a polyhedral convex cone [9]. In [10] a multi-contact robust static balance criterion is proposed. This criterion is simplified in [11] by using the Chebychev center to avoid the direct computation of the region, and by [12] that accelerated the computation by discretization of the friction cones to apply to sliding contacts. These methods do not scale to highly dynamic motions.

| Refs | Human movement target | Assistance criterion |
|---|---|---|
| [1] | Sit-to-stand | Pre-set force |
| [5] | Pre-set arm movement | Torque computed online |
| [6] | Bed transfer | Pre-set trajectory |
| [7] | Wheelchair transfer | Pre-set trajectory |
| Tencent | Wheelchair transfer | Pre-set trajectory |
| Ours | Balanced 3D motions | Balance computed online |

**Table I.** Comparison with some existing methods of humanoid-human physical assistance. All methods apply force control on human except [6] and [7], which use full lifting of human.

### B. Dynamic balance criterion

Several virtual points were successively developed to track dynamic balance in humans and humanoids. The Zero-tilting Moment Point (ZMP) is the point where the accumulated inertia and gravity force cancels the horizontal moment [13]. The Centroidal Moment Pivot (CMP) instead represents the point where a line parallel to the ground reaction force passing through the CoM intersects the contact surface [14]. It provides complementary information about the whole-body rotation dynamics as it accounts for the moments about the CoM (e.g., hip movements [15]), that are not encoded by the ZMP. Controlling both ZMP and CMP enforces balance with non-zero angular momentum, and they coincide when there is none. Yet these centroidal balance methods are less suited for scenarios with vertical CoM motions (e.g., sit-to-stand transitions) because of the coupling between vertical and horizontal CoM dynamics in formulating these points in the linear inverted pendulum model.

To address this, two new points in 3D are proposed in [16]: the extended CMP (eCMP) $\mathbf{r}_{\text{ecmp}}$, and the Virtual Repellent Point (VRP) $\boldsymbol{v}$, separated by a vertical offset $\Delta z$ such that

$$\boldsymbol{v} = \mathbf{r}_{\text{ecmp}} + [0, 0, \Delta z]^T \tag{4}$$

The eCMP generalizes the CMP by allowing it to encode the magnitude of the sum of external forces without being

[1] https://www.age-simulation-suit.com
[2] https://jrl-umi3218.github.io/mc_rtc/index.html

constrained to the ground plane. It is defined as:

$$\mathbf{F}_{\text{ext}} = \frac{m}{b^2}(\boldsymbol{c} - \mathbf{r}_{\text{ecmp}}) \tag{5}$$

$\mathbf{F}_{\text{ext}}$ sums external forces on the CoM, $b = \sqrt{\frac{\Delta z}{g}}$ a constant equivalent to $\frac{1}{\omega_0}$ in other notations, the natural frequency of the inverted pendulum model formed by the CoM and the eCMP.

Adding gravity to the external forces, the VRP $\boldsymbol{v}$ writes:

$$\mathbf{F} = \frac{m}{b^2}(\boldsymbol{c} - \boldsymbol{v}) \tag{6}$$

with $\mathbf{F}$ the total force sum acting on the CoM.

These formulations of the eCMP and VRP allow the CoM dynamics to be decoupled vertically and horizontally, facilitating CoM control for complex movements.

As a last concept for dynamic balance, the Divergent Component of Motion (DCM) $\boldsymbol{\xi}$ combines the CoM pose and velocity such that $\boldsymbol{\xi} = \boldsymbol{c} + b\dot{\boldsymbol{c}}$. In 2D it is also called the capture point [17] or the foot placement estimator (FPE) [18] as it represents the point on the ground where a robot or human should shift its ZMP to come to a stop. The introduction of the eCMP and VRP allowed extending the DCM to 3D and account for vertical movements as well, and its dynamics are:

$$\dot{\boldsymbol{\xi}} = \frac{1}{b}(\boldsymbol{\xi} - \boldsymbol{v}) \tag{7}$$

with $\boldsymbol{\xi}$ diverging away from $\boldsymbol{v}$, keeping the 3D decoupling.

Note that $b$ depends on $\Delta z$; it is introduced to decouple the vertical dynamics from the horizontal one. If only horizontal motions are planned, the average height of the CoM is chosen, placing the VRP at the CoM's height assuming the eCMP is on the ground. As shown in [19], modifying $b$ along movements enables kinematically feasible CoM height variations.

In short, to track the dynamics in decoupled 3D movements we can choose to control the DCM instead of the CoM, using the VRP instead of the ZMP. In this work we apply the same philosophy to infer human balance.

### C. Variable height pendulums and variable VRP offsets

We chose the $\omega$ notation for the $\frac{1}{b}$ coefficient. The 3D DCM with constant height inverted pendulum writes:

$$\boldsymbol{\xi} = \boldsymbol{c} + \frac{1}{\omega_0}\dot{\boldsymbol{c}} \tag{8}$$

$\omega_0 = \sqrt{\frac{g}{\Delta z}}$ is the pendulum frequency, taken constant when the CoM is at a nominal height $\Delta z$. The DCM dynamics is

$$\dot{\boldsymbol{\xi}} = \omega_0(\boldsymbol{\xi} - \boldsymbol{v}) \tag{9}$$

with

$$\boldsymbol{v} = \boldsymbol{c} - \frac{\mathbf{F}_{\text{ext}}}{m\omega_0^2} + [0, 0, \Delta z]^T \tag{10}$$

from (4) and (5). Yet a constant $\Delta z$ means that for a substantial change of the CoM height, the VRP (and so the eCMP) need to move vertically. For a constant $\omega$, this is not possible if one wants to maintain the ground reaction forces, and hence the eCMP, at the contact points. The DCM formulation for a time-varying natural frequency can expand as in [20].

$$\boldsymbol{\xi} = \boldsymbol{c} + \frac{1}{\omega(t)}\dot{\boldsymbol{c}} \tag{11}$$

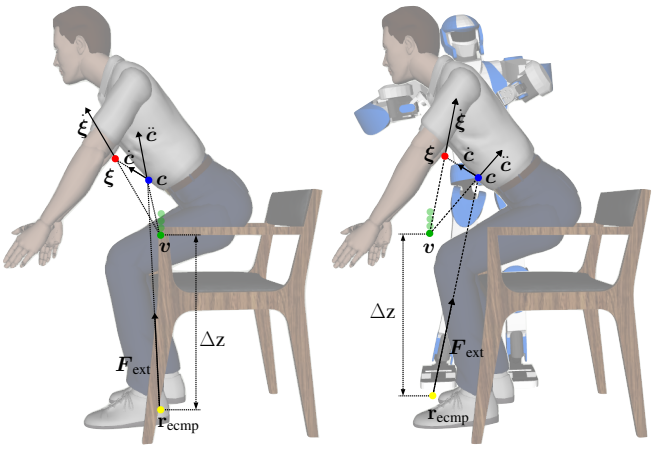


**Figure 2:** Virtual points of interest in the standing motion of a human without any assistance (left), and with humanoid assistance (right).

with $\omega(t) = \sqrt{\frac{g+\ddot{c}_z}{\Delta z(t)}}$ accounting for the CoM vertical acceleration ($\ddot{c}_z$). From now on we use the notation of $\omega$ meaning $\omega(t)$. Differentiating $\boldsymbol{\xi}$ gives:

$$\begin{aligned}\dot{\boldsymbol{\xi}} &= \dot{\boldsymbol{c}} - \frac{\dot{\omega}}{\omega^2}\dot{\boldsymbol{c}} + \frac{1}{\omega}\ddot{\boldsymbol{c}} = \left(\omega - \frac{\dot{\omega}}{\omega}\right)\left(\boldsymbol{\xi} - \left(\boldsymbol{c} - \frac{\ddot{\boldsymbol{c}}}{\omega^2 - \dot{\omega}}\right)\right) \\ &= \left(\omega - \frac{\dot{\omega}}{\omega}\right)(\boldsymbol{\xi} - \boldsymbol{v})\end{aligned} \tag{12}$$

The new expression for $\boldsymbol{v}$ is

$$\boldsymbol{v} = \boldsymbol{c} - \frac{\ddot{\boldsymbol{c}}}{\omega^2 - \dot{\omega}} \tag{13}$$

assuming the CoM linear acceleration $\ddot{\boldsymbol{c}}$ is produced by the gravity and the contact forces, we can write

$$\boldsymbol{v} = \boldsymbol{c} - \frac{\mathbf{F}_{\text{ext}} - m\mathbf{g}}{m(\omega^2 - \dot{\omega})} = \mathbf{r}_{\text{ecmp}} + \frac{\mathbf{g}}{\omega^2 - \dot{\omega}} \tag{14}$$

with the eCMP as

$$\mathbf{r}_{\text{ecmp}} = \boldsymbol{c} - \frac{\mathbf{F}_{\text{ext}}}{m(\omega^2 - \dot{\omega})} \tag{15}$$

In [21] the pendulum's time-varying frequency is defined by a Ricatti equation leading to an input gain for the time variation of $\omega$. The DCM is set by controlling $\omega$ in the internal state (the DCM is 4-dimensional: 3 spatial components and 1 frequencial). Here, as we accompany the human movement, we treat the $\Delta z$ change as a variation of $\omega$ measurable at every time-step. The links between these points are illustrated in Fig. 2 on a person in the same manner as in [19], [20].

## III. Proposed Approach

We apply Sec. II's humanoid balancing knowledge to the assisted person, see Fig. 2. First, we compute the 3D balance region of the person and the required DCM position for the human to be balanced (Sec. III-A). The VRP to steer the DCM to its desired value (Sec. III-C) gives us the wrench to be applied to the human's CoM. Then, the assistive wrench is deduced from either the total measured acceleration at the human's CoM, or from the estimated human external forces. This wrench is distributed among the contacts (Sec. III-D) the

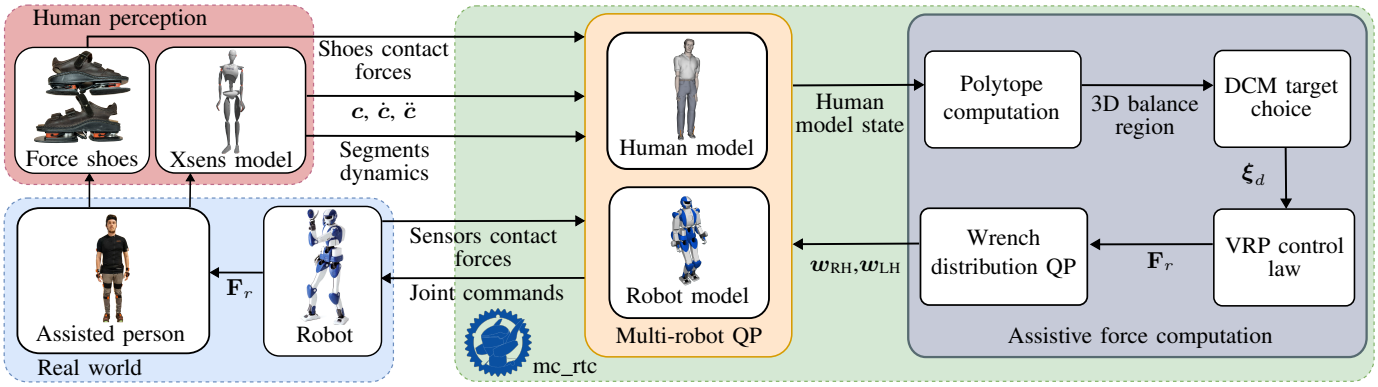


**Figure 3:** All the components of the control system for humanoid assistance of a human.

robot makes on the person and gives us the target for each contact; Fig. 3 illustrates the entire framework.

### A. Generating a reference DCM

The 3D-DCM is a suitable balance indicator for standing and sitting tasks as both involve sagittal and vertical motions. Recent works using the DCM-VRP dynamics still use the projection of the DCM on a 2D balance region [22]. Whereas works leveraging the gravito-inertial wrench cones to generate 3D balance regions use it as a criterion for the CoM position and hence for a quasi-static case [10]–[12]. Instead, we propose using 3D balance regions as a criterion for a 3D-DCM; creating a polytope in which the DCM must lie to guarantee the CoM will converge inside. We compute this polytope using the iterative projection and software proposed in [10], [12]. This results in a dynamic balance criterion that we apply to both agents: human and humanoid. In particular, the human DCM objective $\boldsymbol{\xi}_d$ is set to the current measured DCM $\boldsymbol{\xi}$ if it belongs to the human 3D balance region; otherwise (unbalanced state) the human DCM objective $\boldsymbol{\xi}_d$ is set (by projection) to the closest point belonging to the human 3D balance region. This triggers robot assistance to enforce dynamic balance of the assisted person.

### B. DCM feedback

Generating a VRP reference to achieve $\boldsymbol{\xi}_d$ can be done through feedback control of the DCM [20]. Using (12) we get the VRP value in function of the current measured dynamics:

$$\boldsymbol{v} = \boldsymbol{\xi} - \frac{1}{\omega - \frac{\dot{\omega}}{\omega}}\dot{\boldsymbol{\xi}} \tag{16}$$

The reference VRP $\boldsymbol{v}_r$ (to be applied by the humanoid) is computed as a command law on the DCM error, generated from the human's movements alone. From (16) we have:

$$\boldsymbol{v}_r = \boldsymbol{\xi} - \frac{1}{\omega - \frac{\dot{\omega}}{\omega}}\left[\dot{\boldsymbol{\xi}}_d + \mathbf{k}_P(\boldsymbol{\xi}_d - \boldsymbol{\xi})\right] \tag{17}$$

subscripts $r$ and $d$ mean reference and desired resp.; $\mathbf{k}_P \in \mathbb{R}^{3\times3}$ is a diagonal matrix of the DCM error proportional gain.

### C. Control of the reference VRP

Now, we compare $\boldsymbol{v}_r$ in (17) with the estimated human VRP from the ongoing motion. The VRP discrepancy is corrected by the humanoid applying forces on the human. Equations (13) and (14) offer two ways to determine such a force [23]:

1) by measuring the wrench applied on the human and computing the missing force at the CoM directly; or
2) by measuring the acceleration of the human's CoM, and deducing the force from the missing acceleration.

The first uses (14) and assumes that human CoM acceleration (except gravity) is the result of the sum of environment contact forces $\mathbf{F}_{\text{ext}}$, that is:

$$\ddot{\boldsymbol{c}} = \mathbf{F}_{\text{ext}} - m\mathbf{g} \quad \text{and} \quad \mathbf{F}_{\text{ext}} = \mathbf{F}_r + \mathbf{f}_{\text{LF}} + \mathbf{f}_{\text{RF}} \tag{18}$$

with $\mathbf{F}_r$ the sum of forces applied on the human by the humanoid, and $\mathbf{f}_{\text{LF}}$, $\mathbf{f}_{\text{RF}}$ the individual environment reaction forces at the left and right foot of the person respectively.

From (18) and (13) we deduce the total force to be applied on the person to achieve the desired VRP $\boldsymbol{v}_r$:

$$\begin{aligned} \mathbf{F}_{\text{ext}} &= m(\omega^2 - \dot{\omega})(\boldsymbol{c} - \boldsymbol{v}_r) + m\mathbf{g} \\ \mathbf{F}_r &= m(\omega^2 - \dot{\omega})(\boldsymbol{c} - \boldsymbol{v}_r) + m\mathbf{g} - \mathbf{f}_{\text{LF}} - \mathbf{f}_{\text{RF}} \end{aligned} \tag{19}$$

Note that this is assuming the human makes no other contact than its feet. To handle efficiently contacts for which there is no direct force sensor, see later Sec. IV-B.

If one opts for estimating human's CoM acceleration to determine an acceleration error from the VRP error and deduce the forces to be applied by the robot, we use:

$$\begin{aligned} \ddot{\boldsymbol{c}}_d &= (\omega^2 - \dot{\omega})(\boldsymbol{c} - \boldsymbol{v}_r) \\ \ddot{\boldsymbol{c}}_e &= (\omega^2 - \dot{\omega})(\boldsymbol{c} - \boldsymbol{v}_r) - \ddot{\boldsymbol{c}} \\ \mathbf{F}_r &= m(\omega^2 - \dot{\omega})(\boldsymbol{c} - \boldsymbol{v}_r) - m\ddot{\boldsymbol{c}} \end{aligned} \tag{20}$$

subscripts $d$, and $e$ meaning desired and error respectively.

We get the missing force $\mathbf{F}_r$ to be applied on the human's CoM to achieve the desired VRP.

In fact, the two options use the same equations but the variables measured are different. One can use them in alternate or complementary modes. This combination is possible using complementarity filter, i.e., composition of low pass filtering of the human force model VRP (14) with high pass filtering of the acceleration model VRP (13).

### D. Force distribution

Using either (19) or (20) we formulate a least squares minimization problem to apply the total missing force at the

CoM using both robots 'hands' on the human. The objectives are the sum of contact forces resulting in the total desired force at the CoM, and the minimization of the contacts' moment about the CoM. With $\boldsymbol{w}$ the 6D wrenches, $\mathbf{f}$ the 3D forces, and subscripts LH and RH the left and right hand contact of the robot we have:

$$\begin{aligned} \min_{\boldsymbol{w}_{\text{RH}},\boldsymbol{w}_{\text{LH}}} \quad & ||\mathbf{f}_{\text{RH}} + \mathbf{f}_{\text{LH}} - \mathbf{F}_r||^2 + ||\boldsymbol{w}_{\text{RH}}||^2 + ||\boldsymbol{w}_{\text{LH}}||^2 \\ & + ||(\mathbf{r}_{\text{RH}} - \boldsymbol{c}) \times \mathbf{f}_{\text{RH}} + (\mathbf{r}_{\text{LH}} - \boldsymbol{c}) \times \mathbf{f}_{\text{LH}}||^2 \\ \text{s.t.} \quad & \boldsymbol{w}_{\text{RH}} \in \text{RH contact wrench cone} \\ & \boldsymbol{w}_{\text{LH}} \in \text{LH contact wrench cone} \\ & f_{\text{RH}_z} + f_{\text{LH}_z} < \text{Max total force} \\ & f_{\text{RH}_z} > \text{Min contact force} \\ & f_{\text{LH}_z} > \text{Min contact force} \end{aligned} \tag{21}$$

The contact wrench cone constraints for the hand contacts are formulated as in [24], assuming rigid contacts. The three last constraints on the contacts' normals impose a maximum opposite force on the sum of the contacts to avoid applying uncomfortable forces on the person, and a minimal force to ensure the contacts sustainability during the movement. All of these computations result in the 6D target wrenches for the humanoid's hands. Note that our method is not linked to a particular robot and the assistive forces can be applied by other suitable robotic systems.

## IV. Human Modeling

The assisted human model is added to the task-space multi-robots QP as an additional 'robot' (this was stated as future work in [25]) as follows: (i) human motions are tracked on-line from which the CoM is estimated, e.g., [26]; (ii) human/environment contact forces are obtained on-line from sensors or observed (Sec. IV-B), (iii) persons anthropomorphic data set a URDF human model with inertial parameters, e.g., [27].

### A. Human motion tracking

Reliably estimating human kinematics state (pose and velocity) from on-line video processing is an actively researched problem. While recent works using machine learning show impressive results, e.g., [28], they fail to scale to robotic requirements. Indeed, humanoid embedded perception from a close-human-contact interaction perspective is not precise enough to be used in closed-loop control. To counter this problem temporarily, we opted for motion capture [29] by means of the Xsens motion capture suit; it consists of 17 inertial sensors updated at 60 Hz to continuously monitor the human kinematics. Our controller assumes the human shape and kinematics can be obtained reliably. This functionality is implemented as a standalone module that can be replaced shall humanoid vision-based human tracking become robust.

Let $\boldsymbol{p}_i \in \mathbb{R}^3$ and $\boldsymbol{R}_i \in \mathbb{R}^{3\times3}$ be the translation and rotation of the $i_{\text{th}}$ rigid body, defining its pose $\boldsymbol{r}_i = (\boldsymbol{R}_i, \boldsymbol{p}_i)$. The Xsens units return in real-time the body parts states of the person in the world frame (pose $\boldsymbol{r}$, velocity $\dot{\boldsymbol{r}}$ and acceleration $\ddot{\boldsymbol{r}}$), as well as those related to the human's CoM estimate.

In order to scale the Xsens human model to the measured person we measure the followings: body height, foot length, shoulder height, shoulder width, elbow span, wrist span, arm span (middle finger to middle finger in T pose), hip height, hip width, knee height, ankle height and sole height. Then, a dynamic calibration is performed, requiring the person to walk in line and make a turn to go back to the initial position. This initializes the filters for the `Awinda` motion capture software.

Having all these, human motion can be tracked in the controller by retargeting the body segment measurements from the IMUs to the actuated human model in the multi-robot QP controller. The measured pose $\boldsymbol{r}_d$, velocity $\dot{\boldsymbol{r}}_d$ and acceleration $\ddot{\boldsymbol{r}}_d$ of each body are given as task-space objectives for each body of the human model as follows:

$$\begin{aligned} \ddot{\boldsymbol{r}} &= \ddot{\boldsymbol{r}}_d - \boldsymbol{K}_D \Delta\dot{\boldsymbol{r}} - \boldsymbol{K}_P \Delta\boldsymbol{r} \\ \text{where} \quad \Delta\boldsymbol{r} &= \begin{bmatrix} \Delta\boldsymbol{r}_L \\ \Delta\boldsymbol{r}_A \end{bmatrix} = \begin{bmatrix} \boldsymbol{p} - \boldsymbol{p}_d \\ \ln\left(\boldsymbol{R}\boldsymbol{R}_d^{\mathsf{T}}\right) \end{bmatrix}, \end{aligned} \tag{22}$$

subscript $d$ means desired, subscripts $L$ and $A$ are the linear and angular part of the pose, $\ln(\boldsymbol{R}) \in \mathbb{R}^3$ the operator from rotation matrix to axis angle, and $\boldsymbol{K}_P$, $\boldsymbol{K}_D \in \mathbb{R}^{6\times6}$ proportional and damping matrices, respectively.

This way the human model, scaled to the measured person, reproduces the assisted person's filtered motion. Note that the human (as a 'robot' in the QP) is obviously not controlled, and serves as an observer.

### B. Force observers

If human motion tracking is reliable, [30], [31] showed that it is possible to infer a good estimate of the contact locations and interaction forces from vision alone. In this study, the human is equipped with a pair of Xsens force shoes. Each sole embeds 2 force/moment sensors (ATI-Mini 45) each of which has a linked IMU (one at the heel and one at the toe). These shoes are interfaced through a modified version of the MT Manager software, a proprietary GUI for Xsens devices connected to an Xsens bus. The low level implementation of the MT communication protocol is open[3] but not the high-level MT Manager software, nor the prototype version handling the force sensors. So, we reconstructed the low level protocol for the force sensors. The four devices are linked in a row to an Xbus Master device via a wire, and both shoes are attached to it. This Master device is then linked to a computer running the interface via a bluetooth dongle and sends data packets containing the data sent on the bus by every connected device. Sampled force sensor data is applied at the location of the force sensors on the feet of the human model; this `mc_rtc` plugin is made available[4]. These forces are transformed back to the CoM frame to get the resulting wrench; which is in turn used for the VRP computations (90 Hz) in Sec. III-C.

### C. Controlled human model

Human worn sensors operate at a lower frequencies (60 Hz and 90 Hz) w.r.t our controller (200 Hz). Yet, the human model state is made continuous by interpolating missing measurements using velocity and acceleration objectives to

[3] https://www.movella.com/support/software-documentation
[4] https://github.com/Hugo-L3174/mc_force_shoe_plugin

the retargeting tasks. These objectives are updated when new measurements are received from the sensors.

The human model is a generic template comprising 15 rigid bodies and 34 dof. Each body is controlled by an associate task whose objective is the measured pose of the real person's corresponding body part. This model is dynamically scaled to the Xsens data received online: the kinematic chain for the human is reconstructed from its floating base (the hip). The measured Xsens position of a body is translated in the local frame of the parent link in the model; the rigid body dynamics representation in the controller is updated accordingly. From these modifications we deduce the scaling of each body of the model, allowing also to scale the corresponding convex shapes. The latter are used to build collision constraints in the multi-robot QP: non-desired human-humanoid collisions are enforced using the convex shapes of each model. Desired humanoid-human assistive contacts are guided with feedback of associated force sensors using damping control to softly make contact with the desired surfaces. The position of the end effector is used as reference for the relative position of the body surface, leading to match the morphology of the assisted person. This allows the effective human model's surface to match as closely as possible that of the real person.

## V. Robot Force Control and Balancing

### A. Force control on a moving target

The assistive forces are applied by the robot at desired locations on the person. Position control of the robot end-effectors is made by tracking the task error $\Delta_{\text{EF}}$ in our QP,

$$\Delta_{\text{EF}} = \boldsymbol{K}_P \Delta \boldsymbol{r} + \boldsymbol{K}_D \Delta \dot{\boldsymbol{r}} + \Delta \ddot{\boldsymbol{r}} \tag{23}$$

where $\Delta r$ is defined in (22).

On the other hand, force control is achieved by steering the end-effector from the wrench error following an impedance with mass $\boldsymbol{M}$ spring $\boldsymbol{K}$ damper $\boldsymbol{D}$ system such that

$$\boldsymbol{M}\Delta \ddot{\boldsymbol{r}} + \boldsymbol{D}\Delta \dot{\boldsymbol{r}} + \boldsymbol{K}\Delta \boldsymbol{r} = \boldsymbol{K}_f(\boldsymbol{w}_m - \boldsymbol{w}_d) \tag{24}$$

where $\boldsymbol{w}_m$ and $\boldsymbol{w}_d$ are measured and desired 6D wrenches, respectively. $\boldsymbol{K}_f \in \mathbb{R}^{6\times 6}$ is the gain matrix on the wrench feedback, resulting in the computation of a compliance-frame position, noted $\boldsymbol{r}_{\text{cd}}$, which dynamics is

$$\Delta \ddot{\boldsymbol{r}}_{\text{cd}} = \boldsymbol{M}^{-1}\left(\boldsymbol{K}_f(\boldsymbol{w}_m - \boldsymbol{w}_d) - \boldsymbol{D}\Delta \dot{\boldsymbol{r}}_{\text{cd}} - \boldsymbol{K}\Delta \boldsymbol{r}_{\text{cd}}\right) \tag{25}$$

The gains $\boldsymbol{K}_P, \boldsymbol{K}_D$ in (23) are different from those in (25): the first are the end-effector task's that tracks the position of the person and their dynamics; whereas the latter define the desired behavior of the force control. The latter gains are set from experimental data (high wrench gain to react to small force errors). The compliance acceleration (25), and its integrated compliance velocity and position are added to their respective counterparts in (23). By doing so, and by having the human model in the multi-robot QP, we obtain the desired surfaces's second order dynamics; which is accurately targeted by the end-effector task (23). The position, and first and second order dynamics of this task are then offset following the desired force dynamics (25), ensuring properly applied force at the correct target during the whole movement.

### B. Balancing with external wrenches

Manipulating a human during assistance affects the balance of the humanoid robot. The effects of such manipulation can either be treated as external perturbations or incorporated as prior knowledge [32]. The humanoid is balanced using DCM feedback accounting for the intentional errors induced by the applied external forces. This is notably similar to previous implementations in [33], [34] where the DCM error resulted in a ZMP reference converted to a CoM acceleration command, which in turn resulted in a wrench to be distributed. In contrast, we do not track a 2D ZMP to guide a 2D DCM. Instead, we steer a 3D DCM using a 3D VRP, allowing for free 3D movements of the humanoid CoM, as well as a simple linear relation between the external forces and the VRP (no need to account for the dynamics modification of a pendulum model).

The feedback is translated into a VRP reference command, following the same principles outlined in Sec. III-A. This resultant force is then distributed between the feet contacts using a simple QP, as described in Sec. III-D. While it would be possible to include hand contacts in the distribution of forces across all end-effectors, we treat the hand contacts as planned external perturbations in our current framework.

## VI. Experiments and Results

All the modules described in Fig. 3 are integrated by means of the real-time control framework `mc_rtc`. Prior to an experiment with real persons, we went through two intermediary validation stages. First, the assistance control is thoroughly implemented and tested in simulation using MuJoCo. A human model scaled to each person and the model of three humanoids (the Kawada's HRP-4, the Honda's E2DR and Kawasaki's Friends) are integrated to MuJoCo (Fig. 4). Once worst testing conditions were satisfactory in simulation we moved to the second validation stage.

The second validation step consists in emulating the human's motion using a Panda robotic arm. We attached to its end-effector a cardboard box of the size of a human torso. The Panda plays recorded motion of a real human torso obtained from Xsens tracking (as in simulation). The humanoid (HRP-4) provides assistance to the fake torso and accompanies the Panda emulated motion. All three robots (counting the human as a robot) are running in the same controller. Both physical robots are controlled in real-time and receive commands at their respective frequencies (1 kHz for the Panda arm, 200 Hz for the HRP-4). The controller runs at 5 ms iterations so the movements of the Panda are made continuous by sending acceleration and velocity commands from the QP. The commands are then updated every iteration of the controller and the movements of both robots are continuous, see Fig. 5.

After intensive testing of the Panda experiment repeatability and the safety of the force control, we experimented our assistive controller with three real persons (1 male and 2 females, all labmates). The humanoid HRP-4 is set near each person so it has to position itself w.r.t the person in a few step motions. Then humanoid left and right effectors contacts are made on the person and the human motion tracking starts. All subjects wear the elderly suit emulating the need for more effort and difficulty in standing.

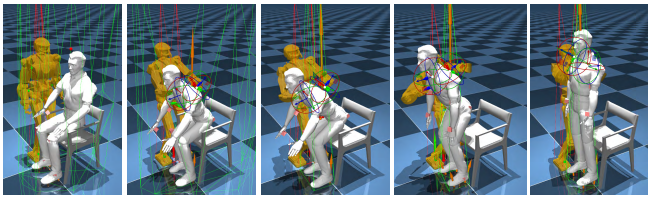

**(a)** Assistance of a person with Kawada Robotics's HRP-4.

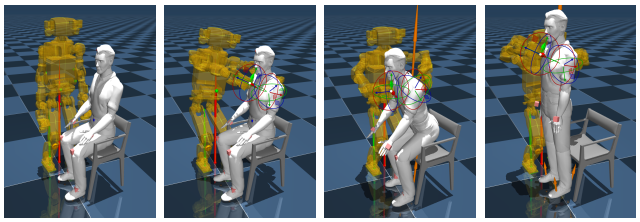

**(b)** Assistance of a person with Honda's E2DR.

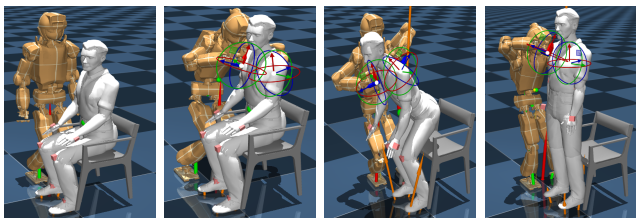

**(c)** Assistance of a person with Kawasaki's Friends.

**Figure 4:** Simulated humanoid-to-human assistance in MuJoCo.

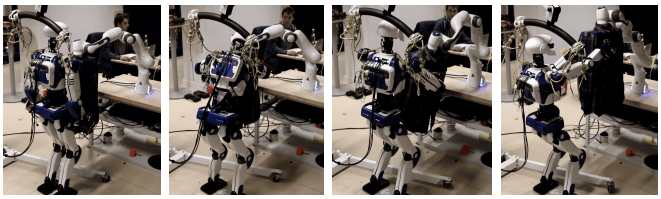

**Figure 5:** Validation with the Panda human-torso motion emulator.

Each person is asked to perform sit-to-stand, followed by stand-to-sit motion after the humanoid makes both supporting contacts on their body. No timing is given, as the person's whole-body dynamics is accounted for, only the person's movement determine if and when assistance is needed.

In fact the motion is dynamically balanced in large parts of the motions. Therefore the subjects are asked to bend up to reach or go out of the balance region limits to show how the assistive control reacts (Fig. 7). In such cases, the computed assistive force is successfully applied as shown in Fig. 6. The tracking is subject to human unforeseeable motions, therefore discrepancies in tracking are unavoidable. Indeed as the human moves, as far as the motion is feasible the applied force drops to near zero (light touch) as the desired offset (5 N) is necessary to track the motion using admittance. Notice that the robot kinematics limitations do not allow to reach the computed desired force in some configurations.

## VII. Discussion

The experiments highlight the importance of designing humanoid robots capable of replicating human motions with similar postural behaviors. A lack of anthropomorphic design could result in postures that significantly deviate from those

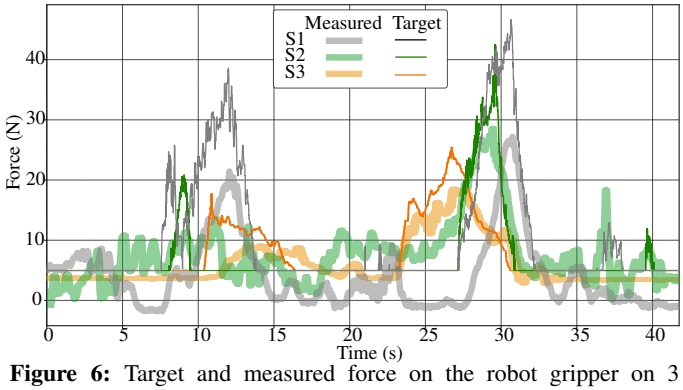


**Figure 6:** Target and measured force on the robot gripper on 3 subjects S1-S3 bending to the limits of their balance region.

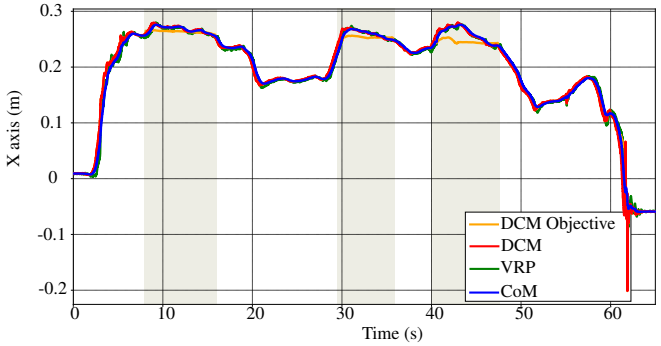


**Figure 7:** Desired and measured DCM of subject 3 bending to the limits of the balance region (light gray areas).

of caregivers, leading to loss of contact during certain configurations due to limited manipulability and range of motion.

While the force tracking could be further optimized, the results indicate that the amount of assistive force applied is relatively small, with no saturation of the forces. We hypothesize that this is not due to the specific movements of any one subject, but rather a reflection of the forces required to assist frail individuals. In this context, the role of the humanoid is likely not to provide high forces, but rather to act as a reconfigurable aid, offering the user the ability to select the most appropriate supporting contact for their motion. Additionally, we hypothesize that a person's engagement behavior would differ when a contact is present, even if no force is applied by the robot, as shown in previous studies (e.g., [35]). To explore this further, we plan to conduct specific human studies, as these results could influence the way human-robot physical interaction is approached in assistive technologies.

Ethical clearance is required to conduct experiments with frail individuals, and most existing humanoid robots are not yet certified for physical interaction. However, we hope that the current experiments demonstrate how certain safety guarantees can be achieved, potentially serving as a milestone toward obtaining research-specific clearance for such studies.

The computation of the balance region also remains an area for improvement (ongoing work). The current model assumes that a person can place their entire weight on a single contact point, which may not be accurate for frail or impaired individuals. Incorporating data on human articulation torque limitations could enhance the accuracy of the dynamic balance region calculations. This data could potentially be

gathered from repeated experiments when the balance region is violated. Moreover, the assistive force could be computed using a damped DCM before reaching the boundaries of the balance region. While this implementation would likely lead to more conservative assistance, it would also provide a safer, more proactive approach to assisting individuals in motion.

## VIII. Conclusion

This letter presents a framework for assisting frail or impaired individuals using a humanoid robot. The system evaluates the assisted person's balance in real-time to calculate the necessary assistive forces, enabling the robot to provide support while ensuring safe, close interactions. By utilizing the 3D DCM-VRP relationship, the framework can balance both the humanoid robot and the human user simultaneously, demonstrating how advancements in humanoid design can be effectively applied to analyze and support human movement.

Our framework is applicable to scenarios involving any number of non-coplanar contacts. Future work will focus on conducting broader human studies to better understand the forces required for assistance, improving the balance region computation, and exploring more complex assistive cases, including contact switching by the humanoid during assistance.

## References


[1] A. M. López, J. Vaillant, F. Keith, P. Fraisse, and A. Kheddar, "Compliant control of a humanoid robot helping a person stand up from a seated position," in *IEEE-RAS International Conference on Humanoid Robots*, 2014, pp. 817–822.

[2] A. Bolotnikova, S. Courtois, and A. Kheddar, "Multi-contact planning on humans for physical assistance by humanoid," *IEEE Robotics and Automation Letters*, vol. 5, no. 1, pp. 135–142, 2020.

[3] Z. Aftab, T. Robert, and P.-B. Wieber, "Balance recovery prediction with multiple strategies for standing humans," *PLOS ONE*, vol. 11, no. 3, pp. 1–16, 03 2016.

[4] C. Z. Qiao, A. M. Nasrabadi, R. Partovi, P. Belzner, C. Kuo, L. C. Wu, and J.-S. Blouin, "Multidirectional human-in-the-loop balance robotic system," *IEEE Robotics and Automation Letters*, vol. 8, no. 7, pp. 3948–3955, 2023.

[5] A. Bolotnikova, S. Courtois, and A. Kheddar, "Adaptive task-space force control for humanoid-to-human assistance," *IEEE Robotics and Automation Letters*, vol. 6, no. 3, pp. 5705–5712, 2021.

[6] T. Mukai, S. Hirano, H. Nakashima, Y. Kato, Y. Sakaida, S. Guo, and S. Hosoe, "Development of a nursing-care assistant robot riba that can lift a human in its arms," in *IEEE/RSJ International Conference on Intelligent Robots and Systems*, 2010, pp. 5996–6001.

[7] H. Iwata and S. Sugano, "Design of human symbiotic robot twendy-one," in *IEEE International Conference on Robotics and Automation*, 2009, pp. 580–586.

[8] T. Bretl and S. Lall, "Testing static equilibrium for legged robots," *IEEE Transactions on Robotics*, vol. 24, no. 4, pp. 794–807, 2008.

[9] S. Caron, Q.-C. Pham, and Y. Nakamura, "Leveraging cone double description for multi-contact stability of humanoids with applications to statics and dynamics," in *Robotics: Science and System*, 2015.

[10] H. Audren and A. Kheddar, "3-D robust stability polyhedron in multi-contact," *IEEE Transactions on Robotics*, vol. 34, no. 2, pp. 388–403, 2018.

[11] S. Samadi, J. Roux, A. Tanguy, S. Caron, and A. Kheddar, "Humanoid control under interchangeable fixed and sliding unilateral contacts," *IEEE Robotics and Automation Letters*, vol. 6, no. 2, pp. 4032–4039, 2021.

[12] J. Roux, S. Samadi, E. Kuroiwa, T. Yoshiike, and A. Kheddar, "Control of humanoid in multiple fixed and moving unilateral contacts," in *International Conference on Advanced Robotics*, 2021, pp. 793–799.

[13] P. Sardain and G. Bessonnet, "Forces acting on a biped robot. center of pressure-zero moment point," *IEEE Transactions on Systems, Man, and Cybernetics - Part A: Systems and Humans*, vol. 34, no. 5, pp. 630–637, 2004.

[14] M. Popovic, A. Goswami, and H. Herr, "Ground reference points in legged locomotion: Definitions, biological trajectories and control implications," *The International Journal of Robotics Research*, vol. 24, pp. 1013–1032, 12 2005.

[15] B. J. Stephens and C. G. Atkeson, "Dynamic balance force control for compliant humanoid robots," in *IEEE/RSJ International Conference on Intelligent Robots and Systems*, 2010, pp. 1248–1255.

[16] J. Englsberger, C. Ott, and A. Albu-Schäffer, "Three-dimensional bipedal walking control based on divergent component of motion," *IEEE Transactions on Robotics*, vol. 31, no. 2, pp. 355–368, 2015.

[17] J. Pratt, J. Carff, S. Drakunov, and A. Goswami, "Capture point: A step toward humanoid push recovery," in *IEEE-RAS International Conference on Humanoid Robots*, 2006, pp. 200–207.

[18] L. H. Sloot, M. Millard, C. Werner, and K. Mombaur, "Slow but steady: similar sit-to-stand balance at seat-off in older vs. younger adults," *Frontiers in Sports and Active Living*, vol. 2, 2020.

[19] G. Mesesan, R. Schuller, J. Englsberger, C. Ott, and A. Albu-Schäffer, "Unified motion planner for walking, running, and jumping using the three-dimensional divergent component of motion," *IEEE Transactions on Robotics*, vol. 39, no. 6, pp. 4443–4463, 2023.

[20] M. A. Hopkins, D. W. Hong, and A. Leonessa, "Humanoid locomotion on uneven terrain using the time-varying divergent component of motion," in *IEEE-RAS International Conference on Humanoid Robots*, 2014, pp. 266–272, iSSN: 2164-0580.

[21] S. Caron, A. Escande, L. Lanari, and B. Mallein, "Capturability-based pattern generation for walking with variable height," *IEEE Transactions on Robotics*, vol. 36, no. 2, pp. 517–536, 2020.

[22] G. Zambella, R. Schuller, G. Mesesan, A. Bicchi, C. Ott, and J. Lee, "Agile and dynamic standing-up control for humanoids using 3d divergent component of motion in multi-contact scenario," *IEEE Robotics and Automation Letters*, vol. 8, no. 9, pp. 5624–5631, 2023.

[23] S. Wang, G. Mesesan, J. Englsberger, D. Lee, and C. Ott, "Online virtual repellent point adaptation for biped walking using iterative learning control," in *IEEE-RAS International Conference on Humanoid Robots*, 2021, pp. 112–119.

[24] S. Caron, Q.-C. Pham, and Y. Nakamura, "Stability of surface contacts for humanoid robots: Closed-form formulae of the contact wrench cone for rectangular support areas," in *IEEE International Conference on Robotics and Automation*, 2015, pp. 5107–5112.

[25] K. Bouyarmane, K. Chappellet, J. Vaillant, and A. Kheddar, "Quadratic programming for multirobot and task-space force control," *IEEE Transactions on Robotics*, vol. 35, no. 1, pp. 64–77, 2019.

[26] J. Carpentier, M. Benallegue, N. Mansard, and J.-P. Laumond, "Center-of-mass estimation for a polyarticulated system in contact—a spectral approach," *IEEE Transactions on Robotics*, vol. 32, no. 4, pp. 810–822, 2016.

[27] J. Jovic, A. Escande, K. Ayusawa, E. Yoshida, A. Kheddar, and G. Venture, "Humanoid and human inertia parameter identification using hierarchical optimization," *IEEE Transactions on Robotics*, vol. 32, no. 3, pp. 726–735, 2016.

[28] G. Lan, Y. Wu, F. Hu, and Q. Hao, "Vision-based human pose estimation via deep learning: A survey," *IEEE Transactions on Human-Machine Systems*, vol. 53, no. 1, p. 253–268, Feb. 2023.

[29] C. Gu, W. Lin, X. He, L. Zhang, and M. Zhang, "Imu-based motion capture system for rehabilitation applications: A systematic review," *Biomimetic Intelligence and Robotics*, vol. 3, no. 2, p. 100097, 2023.

[30] T.-H. Pham, N. Kyriazis, A. A. Argyros, and A. Kheddar, "Hand-object contact force estimation from markerless visual tracking," *IEEE Transactions on Pattern Analysis and Machine Intelligence*, vol. 40, no. 12, pp. 2883–2896, 2018.

[31] T.-H. Pham, S. Caron, and A. Kheddar, "Multicontact interaction force sensing from whole-body motion capture," *IEEE Transactions on Industrial Informatics*, vol. 14, no. 6, pp. 2343–2352, 2018.

[32] M. Murooka, K. Chappellet, A. Tanguy, M. Benallegue, I. Kumagai, M. Morisawa, F. Kanehiro, and A. Kheddar, "Humanoid loco-manipulations pattern generation and stabilization control," *IEEE Robotics and Automation Letters*, vol. 6, no. 3, pp. 5597–5604, 2021.

[33] S. Caron, A. Kheddar, and O. Tempier, "Stair climbing stabilization of the HRP-4 humanoid robot using whole-body admittance control," in *IEEE International Conference on Robotics and Automation*, 2019, pp. 277–283.

[34] M. Murooka, M. Morisawa, and F. Kanehiro, "Centroidal trajectory generation and stabilization based on preview control for humanoid multi-contact motion," *IEEE Robotics and Automation Letters*, vol. 7, no. 3, pp. 8225–8232, Jul. 2022.

[35] J. J. Jeka, "Light touch contact as a balance aid," *Physical therapy*, vol. 77, no. 5, pp. 476–487, 1997.